2017-01-01

Chromium poisoning effects on performance of (La, Sr) MnO3-based cathode...

Chromium Poisoning Effects on Performance of (La,Sr)MnO_3-Based Cathode in Anode-Supported Solid Oxide Fuel Cells

Ruofan Wang,[a] Uday B. Pal,[a,b,*,z] Srikanth Gopalan,[a,b] and Soumendra N. Basu[a,b]

[a]*Division of Materials Science and Engineering, Boston University, Brookline, Massachusetts 02446, USA*
[b]*Department of Mechanical Engineering, Boston University, Boston, Massachusetts 02215, USA*

Chromium (Cr) vapor species from chromia-forming alloy interconnects are known to cause cathode performance degradation in solid oxide fuel cells (SOFCs). To understand the impact of Cr-poisoning on cathode performance, it is important to determine its effects on different cathode polarization losses. In this study, anode-supported SOFCs, with a (La,Sr)MnO_3 (LSM) + yttria-stabilized zirconia (YSZ) cathode active layer and a LSM cathode current collector layer were fabricated. At 800°C, cells were electrochemically tested in direct contact with Crofer22H meshes, under different cathode atmospheres (dry air or humidified air) and current conditions (open-circuit or galvanostatic). Significant performance degradation was observed when cell was tested under galvanostatic condition (0.5 A/cm^2), which was not the case under open-circuit condition. Humidity was found to accelerate the performance degradation. By curve-fitting the experimentally measured current-voltage traces to a polarization model, the effects of Cr-poisoning on different cathodic polarization losses were estimated. It is found that, under normal operating conditions, increase of activation polarization dominates the cathode performance degradation. Microstructures of the cathodes were characterized and Cr-containing deposits were identified. Higher concentrations of Cr-containing deposits were found at the cathode/electrolyte interface and the amounts directly correlated with the cell performance degradations.

Manuscript submitted March 22, 2017; revised manuscript received April 26, 2017. Published May 5, 2017.

Performance degradation during long-term operation is one of the major challenges that needs to be overcome for successful commercialization of solid oxide fuel cells (SOFCs).[1–3] At SOFC operating temperature, chromium (Cr) vapor species that evaporate over chromia-forming alloy interconnect, can transport and deposit within the cathode and thereupon cause degradation of the cathode performance.[4–7] Cr-poisoning has been studied extensively on (La,Sr)MnO_3 (LSM)-based cathode. Taniguchi et al. reported that Cr moves to cathode/electrolyte interface by cathodic current, and cathode polarization increases in correlation with the intensity of chromium at the interface.[8] Konysheva et al.[9] and Bentzen et al.[10] observed that Cr-containing deposits can fill up the pores close to the cathode/electrolyte interface and extend into the bulk cathode. Krumpelt et al. found that both the amount of Cr deposition and the rate of performance degradation increase with increasing current density.[11]

For understanding the effects of Cr-poisoning on the cathode performance, it is important to identify what is the most affected cathode process, namely, the nature of the polarization loss in the cathode. To separate the contributions of various polarization losses, deconvolution of the impedance spectra data into equivalent circuit model is usually performed.[12,13] Matsuzaki and Yasuda analyzed the impedance spectra using a Randles-type equivalent circuit and found that both charge transfer and surface diffusion resistance increased due to Cr-poisoning.[14] Kornely et al. used the distribution of relaxation times (DRT) method to separate the impedance spectra into single loss contributions, and they discovered that the process which couples oxygen surface exchange at the triple phase boundaries (TPB's) and oxygen ion diffusion in the bulk cathode was impacted by Cr-poisoning.[15] However, it can be difficult to interpret the information from impedance spectra (especially of anode-supported cells), since the correlation between the equivalent circuit elements and the physical or chemical parameters are not straightforward.[16,17] Furthermore, impedance spectra do not always correspond to the actual cell performance, which will be discussed hereinafter (in section Electrochemical impedance spectroscopy under open-circuit condition).

In the present work, we propose to evaluate the Cr-poisoning effects by modeling and analyzing the current-voltage (C-V) measurements. Anode-supported SOFCs with LSM-based cathode in contact with chromia-forming interconnect (Crofer22H), were electrochemically tested at 800°C. On identical cells, test conditions were varied and different extents of performance degradation were observed. The current-voltage (C-V) traces measured with and without Cr-poisoning effects were curve-fitted to an analytical polarization model. Polarization losses associated with different cathode processes were successfully evaluated and compared. Polarization loss that is closely correlated with the effect of Cr-poisoning is determined, and a physical interpretation of this effect is proposed to help understand the mechanism of cathode performance degradation.

Experimental

Cell fabrication.—In this study, commercially available cell structures (Materials and Systems Research Inc., USA) consisting of a Ni/8YSZ (8 mol% Y_2O_3–92 mol% ZrO_2) anode substrate, a Ni/8YSZ anode interlayer and an 8YSZ electrolyte, were employed. The NiO:YSZ weight ratio was 50:50 in both anode substrate and anode interlayer before cell reduction. The thicknesses of anode substrate, anode interlayer and electrolyte are approximately 750 μm, 10 μm and 8 μm, respectively. The approximate area of anode (and electrolyte) was 7.3 cm^2. A LSM/8YSZ composite cathode active layer and a LSM cathode current collector layer were applied over the 8YSZ electrolyte by screen printing. Cathode active layer slurry was prepared by mixing $(La_{0.8}Sr_{0.2})_{0.95}MnO_{3-\delta}$ (Fuel Cell Materials, USA) and 8YSZ (Tosoh Corp., Japan) powders in 50:50 wt% and ball milling for 10 hours in alpha-terpineol (Alfa Aesar, USA) with the desired amount of pore former (Carbon lampblack, Fisher Scientific, USA) and binder (V6, Heraeus, USA). Cathode current collector layer slurry was prepared by mixing overnight $(La_{0.8}Sr_{0.2})_{0.95}MnO_{3-\delta}$ powder with the desired amount of pore former (Carbon black, Fisher Scientific, USA) and binder (V6, Heraeus, USA) in alpha-terpineol. Zirconia balls with diameter of 10 mm (Tosoh Corp. Japan) were used as grinding media for preparing the slurries of cathode layers. After screen printing of each layer, the cell structure was sintered at 1200°C for 2 hours. After sintering, the thicknesses of cathode active layer and cathode current collector layer were approximately 30 μm and 50 μm, respectively. The approximate cathode area was 2 cm^2.

Cell testing.—Crofer22H (Fe-Cr-Mn alloy) was used as the interconnect material in this work.[18] Crofer22H mesh with mesh opening of about 0.6 × 0.9 mm and thickness of 0.2 mm, was commercially

*Electrochemical Society Member.
[z]E-mail: upal@bu.edu

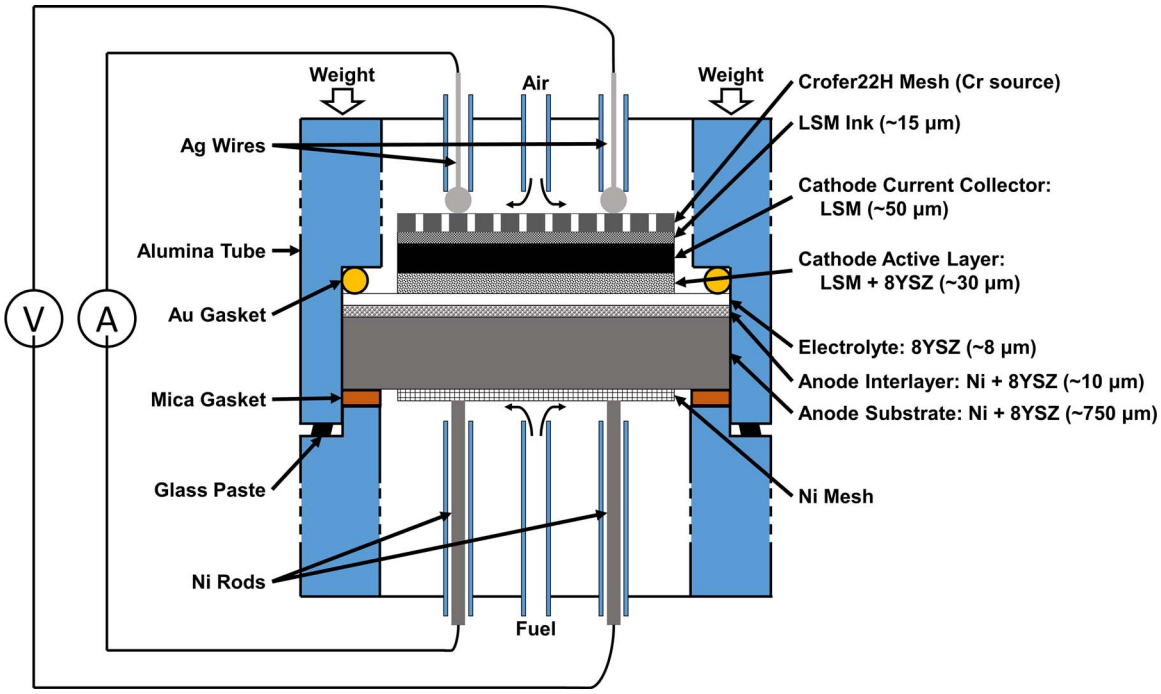

Figure 1. Schematic of setup for cell testing.

purchased from Fiaxell Sàrl (Switzerland). As part of the cell assembly, the Crofer22H mesh was cut into round shape having the same area as the cathode (2 cm^2), and was attached on the cathode with LSM ink (a LSM slurry and polyvinyl butyral mixture) for current collection. A Ni mesh was also pre-attached on the anode with Ni ink (Fuel Cell Materials, USA). Figure 1 shows the schematic of the setup for cell testing. It is comprised of two alumina tubes, with the cell sandwiched between them. Two silver wires with silver beads on the ends were pressed (by spring loading of less than 0.5 kg) on the Crofer22H mesh to serve as current and voltage probes on the cathode side, and two Ni rods were pressed on the Ni mesh to serve as current and voltage probes on the anode side. A gold gasket (Scientific Instrument Services, Inc., USA) on the cathode side and a mica gasket (Fuel Cell Materials, USA) on the anode side were compressed by spring loading of approximately 5 kg to obtain gas tightness. In addition, glass paste (Fuel Cell Store, USA) was applied outside the alumina tubes around the mating circumference to ensure a tight seal.

The cells were electrochemically tested at 800°C. In order to simulate low fuel utilization condition, 98% H_2 – 2% H_2O was circulated over the anode (obtained by bubbling H_2 through a water bath at ~18°C). The fuel flow rate was 300 cm^3/min, which provided a flooded fuel condition and negligible fractional fuel utilization. Initially, dry air was circulated over the cathode at a flow rate of 1000 cm^3/min (with gas velocity of approximately 4.8 m/s at 800°C), also providing a flooded condition with negligible fractional oxidant utilization. The cells were first operated under open-circuit condition for at least 48 hours so that the cells could equilibrate. Galvanostatic pretreatment process prior to actual cell testing was not suitable in this experiment because it would cause undesired Cr-related degradation prior to the actual measurements. After the cell performances became stable under open-circuit condition, the initial performances of the cells were characterized by current-voltage (C-V) measurements and electrochemical impedance spectroscopy (EIS).

After the initial performance measurements, different cathode atmospheres and current conditions were imposed on identical cells (from the same batch); the details of cell tests are shown in Table I. Dry air was obtained by passing compressed air through desiccant, and 10% humidified air was obtained by passing the dry air through a water bubbler maintained at 46°C (the gas tubing for the humidified air was heated to prevent condensation of the water vapor). In order to characterize the cell performance as a function of time, the open-circuit condition for Cell A/C or galvanostatic condition for Cell B/D was interrupted for making the C-V and EIS measurements every 24 hours. Subsequently, C-V and EIS measurements were made on these cells with a dry air cathode atmosphere and the cell performances were evaluated. This provided a consistent cathode atmosphere of dry air for comparing the performances of Cell A, B, C, and D. A Princeton Applied Research PARSTAT® 2273 potentiostat and a KEPCO BOP 20-20M power amplifier were used for all electrochemical measurements.

Table I. Cell test conditions imposed on four identical cells.

Cell	Cathode Atmosphere	Current Condition	Duration (h)
Cell A	Dry air	Open-circuit	120
Cell B	Dry air	Galvanostatic (0.5 A/cm^2)	120
Cell C	10% Humidified air	Open-circuit	120
Cell D	10% Humidified air	Galvanostatic (0.5 A/cm^2)	120

Microstructure characterization.—After electrochemical testing, cells were fractured and sputter-coated with carbon. The cross-sectional microstructures of the cells were observed using a field emission scanning electron microscopy (SEM, Zeiss Supra 55VP). The energy-dispersive X-ray spectroscopy (EDX) was used to perform elemental analysis (EDAX, USA).

Results and Discussion

Current-voltage measurements.—Figure 2 shows the C-V curves and the corresponding power density data of the four cells operated under different cathode atmospheres and current conditions. The initial maximum power densities of these four cells (measured under the same initial dry air and open-circuit condition) were very close (0.45±0.02 W/cm^2), indicating consistent initial cell performances (see Figure 2 for 0 h test results). However, after different cell operating conditions were imposed, different degradation behaviors of cell

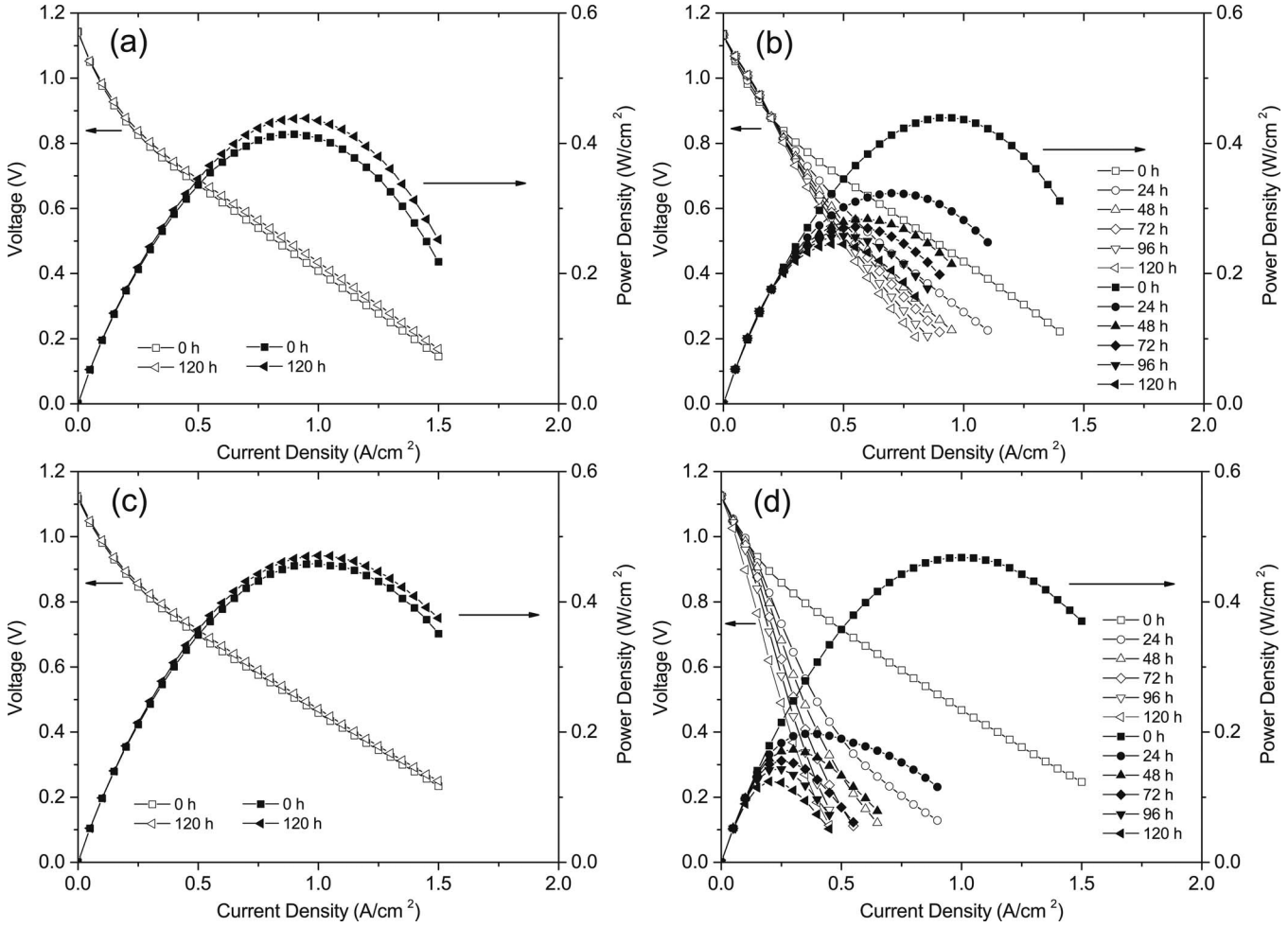

Figure 2. Electrochemical test results of (a) Cell A, (b) Cell B, (c) Cell C, and (d) Cell D.

performances were observed from the C-V curves, and they can be described as follows:

(a) Cell A, which was operated under open-circuit condition with dry air flowing over the cathode, had no observable performance degradation (see Figure 2a). The initial maximum power density of this cell was 0.43 W/cm^2, and that after 120 hours was 0.44 W/cm^2. The slight improvement of cell performance may be associated with the cell break-in, since no pre-treatment was performed.

(b) Cell B was also tested in a dry air cathode atmosphere. Unlike Cell A, Cell B was operated under a constant cathodic current density of 0.5 A/cm^2 after the initial performance was measured. Significant degradation of the cell performance was observed (see Figure 2b). The maximum power densities decreased as follows: 0.44 W/cm^2 (0 h), 0.32 W/cm^2 (24 h), 0.28 W/cm^2 (48 h), 0.27 W/cm^2 (72 h), 0.26 W/cm^2 (96 h) and 0.25 W/cm^2 (120 h). The cell performance degraded rapidly during the first 24 hours of the imposed galvanostatic condition. After the rapid initial degradation, the rate of degradation decreased. In total, the maximum power density of Cell B decreased by approximately 43% in 120 hours.

(c) Cell C was operated under open-circuit condition with 10% humidified air over the cathode. Similar to Cell A, no performance degradation of Cell C was observed (see Figure 2c). The maximum power density of this cell increased from 0.46 W/cm^2 at 0 hour to 0.47 W/cm^2 at 120 hours (reason same as in (a)).

(d) Cell D was tested in an extreme condition: under a constant cathodic current density of 0.5 A/cm^2 with 10% humidified air over the cathode. A dramatic degradation of cell performance was observed in the first 24 hours, followed by a steady deterioration. The maximum power densities decreased as follows: 0.47 W/cm^2 (0 h), 0.20 W/cm^2 (24 h), 0.17 W/cm^2 (48 h), 0.16 W/cm^2 (72 h), 0.14 W/cm^2 (96 h) and 0.12 W/cm^2 (120 h). Overall, the maximum power density of Cell D decreased by approximately 74% in 120 hours.

Electrochemicals impedance spectroscopy under open-circuit condition.—Figure 3a, 3b, 3c and 3d show the impedance spectra of Cell A, B, C and D measured under open-circuit condition at 800°C, respectively. In an impedance spectrum, the high-frequency intercept on the real axis corresponds to the ohmic resistance (R_Ω) of the cell, interconnect and lead wires. The low-frequency intercept on the real axis corresponds to the total resistance (R_{tot}) including ohmic resistance, activation polarization resistance, and concentration polarization resistance. Therefore, the sum of the activation and concentration polarization resistances, R_p, can be obtained by subtracting the high-frequency intercept from the low-frequency intercept on the real axis.[19–21] The results of EIS measurements can be described as follows:

(a) In these four cells, no significant changes of ohmic resistances were found, indicating that the cathode performance degradation caused by Cr-poisoning is not due to the increase in the ohmic resistance. The stable area specific ohmic resistances of these four cells also indicate that the oxide scales formed over the Crofer22H meshes did not have significant differences in thickness,

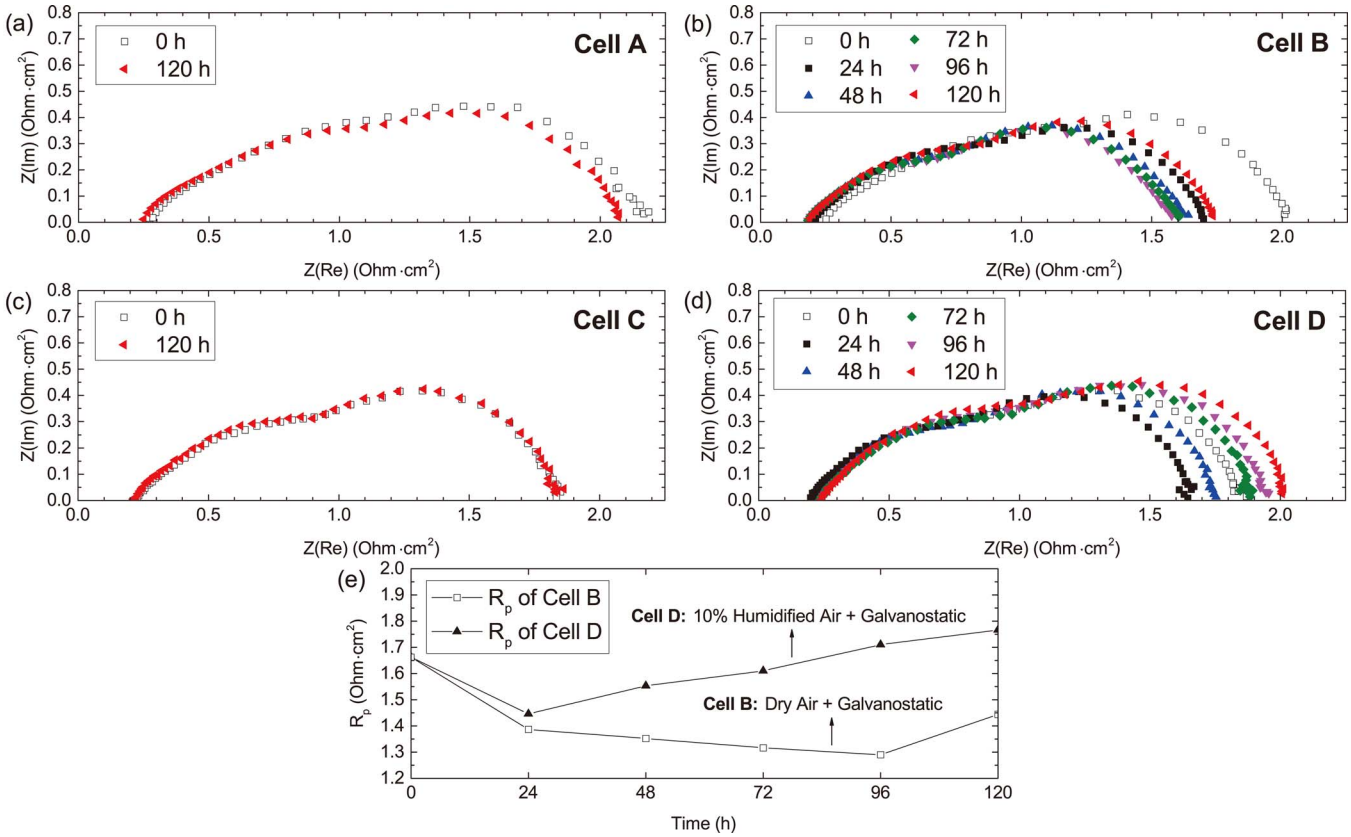

Figure 3. Impedance spectra of (a) Cell A, (b) Cell B, (c) Cell C, and (d) Cell D measured under open-circuit condition at 800°C. (e) Time dependences of polarization resistances (R_p) for Cell B and Cell D (obtained from the impedance spectra).

microstructure and chemical composition after the 120-h testing under different cathode atmospheres and current conditions.

(b) When there was no galvanostatic condition imposed on the cells (Cell A and C), R_p showed slight decrease (Figure 3a) or no change (Figure 3c), which corresponds to the stable cell performances characterized by C-V measurements.

(c) When galvanostatic condition (0.5 A/cm^2) was imposed on the cells (Cell B and D), different behavior was observed on R_p (see Figures 3b and 3d). R_p of Cell B (which was operated in dry air) decreased for the first 96 hours, but the rate of decrease in the first 24 hours was more rapid. R_p of Cell D (which was operated in 10% humidified air) decreased in the first 24 hours and then increased with time. The time dependences of R_p's for Cell B and D are normalized and plotted in Figure 3e.

In the case of Cell B and D, the magnitude of degradation (increase in R_p) and the time when degradation started to occur were different between EIS (Figure 3) and C-V (Figure 2) measurements. The behavior that R_p decreases initially and then increases was also observed by some other authors.[4,14,22,23] Matsuzaki and Yasuda explained it to be due to the partial recovery of the electrode performance after switching off the current.[14] Jiang el al. observed that the decrease of R_p was much more moderate in the presence of chromia-forming alloy, compared with that in the absence of chromia-forming alloy.[22] In our case, it was found that the decrease of R_p lasted for a much shorter time in Cell D (24 h) than in Cell B (96 h). Considering that no pre-treatment was performed before any electrochemical measurements, we ascribe the initial decrease of the R_p to the activation effect of cathodic current on cell performance,[22,24] and it was captured by impedance spectroscopy under open-circuit condition. This activation effect was counteracted by the detrimental effect of Cr-poisoning which was larger in Cell D than in Cell B. From these measurements, it is confirmed that the impedance measured under open-circuit condition do not always reflect the actual performance degradation caused by Cr-poisoning.

Polarization modeling.—In section Electrochemical impedance spectroscopy under open-circuit condition, it has been discussed that impedance spectra measured under open-circuit condition do not fully correspond to the Cr-poisoning effects on the actual cell performance characterized by C-V measurement. In order to evaluate the effects of Cr-poisoning on individual polarization losses, a polarization model developed earlier was employed for analyzing the C-V measurement characteristics.[17,21,25,26] This polarization model is based on a potential balance equation which relates the operating cell potential (V_{cell}) to the open-circuit potential (V_o) and various polarization (ohmic, activation, and concentration) losses

$$V_{cell} = V_o - iR_i - \eta_{act} - \eta_{conc,a} - \eta_{conc,c} \quad [1]$$

where i is the current density (A/cm^2), R_i is the area specific ohmic resistance of the cell ($\Omega \cdot cm^2$) which consists of the contributions of electrolyte, electrodes and contacts, η_{act} is the activation polarization (V), $\eta_{conc,a}$ is the anodic concentration polarization (V), and $\eta_{conc,c}$ is the cathodic concentration polarization (V).

Activation polarization, η_{act}, is caused by slow charge transfer reactions between the electronic and ionic conductors at the triple phase boundaries. For small currents or rapid mass transfer, η_{act} is related to the current density by the Butler-Volmer equation

$$i = i_o \exp\left(\frac{\alpha n \eta_{act} F}{RT}\right) - i_o \exp\left(\frac{(1-\alpha) n \eta_{act} F}{RT}\right) \quad [2]$$

where i_o is exchange current density (A/cm^2), α is the transfer coefficient, n is the number of electrons transferred per reaction, F is Faraday constant, R is the gas constant, and T is the cell operating temperature. n can be 1 or 2 depending on the reaction mechanism, and n = 1 was found to provide a better fit to the polarization model

in this study. α is set equal to 0.5 with the assumption of a symmetric activation energy barrier for the fuel cell application.[21,27] Thus, activation polarization, η_{act}, can be expressed as[21,28,29]

$$\eta_{act} = \frac{2RT}{F}\ln\left\{\frac{1}{2}\left[\left(\frac{i}{i_o}\right)+\sqrt{\left(\frac{i}{i_o}\right)^2+4}\right]\right\} \quad [3]$$

In Equation 3, the activation polarizations occurring at both the cathode ($\eta_{act,c}$) and the anode ($\eta_{act,a}$) are lumped together.

Concentration polarization, η_{conc}, is caused by slow mass transport of gaseous reactants and product species through the porous anode and cathode. The electrode process can be dominated by the concentration polarization at high current densities and/or when the porosity is insufficient for mass transport. The anodic concentration polarization, $\eta_{conc,a}$, with H_2-H_2O gas mixture as fuel in this study, can be expressed as[17,25,26]

$$\eta_{conc,a} = -\frac{RT}{2F}\ln\left(\frac{p^{(i)}_{H_2}p^{o}_{H_2O}}{p^{o}_{H_2}p^{(i)}_{H_2O}}\right) = -\frac{RT}{2F}\ln\left(1-\frac{i}{i_{as}}\right)+\frac{RT}{2F}\left(1+\frac{p^{o}_{H_2}i}{p^{o}_{H_2O}i_{as}}\right) \quad [4]$$

where $p^{(i)}_{H_2}$ and $p^{(i)}_{H_2O}$ are the partial pressure of H_2(g) and H_2O(g) at the anode/electrolyte interface, respectively, $p^{o}_{H_2}$ and $p^{o}_{H_2O}$ are the partial pressure of H_2(g) and H_2O(g) outside the anode surface, respectively, and i_{as} is the anodic saturation current density. The anodic saturation current density is the current density at which the $p^{(i)}_{H_2}$ becomes zero.

The cathodic concentration polarization, $\eta_{conc,c}$, with air (O_2 and N_2 mixture) as oxidant, can be expressed as[17,25,26]

$$\eta_{conc,c} = -\frac{RT}{4F}\ln\left(\frac{p^{(i)}_{O_2}}{p^{o}_{O_2}}\right) = -\frac{RT}{4F}\ln\left(1-\frac{i}{i_{cs}}\right) \quad [5]$$

where $p^{(i)}_{O_2}$ is the partial pressure of oxygen at the cathode/electrolyte interface, $p^{o}_{O_2}$ is the partial pressure of oxygen outside the cathode surface, and i_{cs} is cathodic saturation current density. The cathodic saturation current density is the current density at which the $p^{(i)}_{O_2}$ becomes zero.

Finally, by substituting Equations 3, 4, and 5 into Equation 1, the relationship between the operating cell potential (V_{cell}) and the current density (i) can be obtained[17,25,26]

$$V_{cell}(i) = V_o - iR_i - \frac{2RT}{F}\ln\left\{\frac{1}{2}\left[\left(\frac{i}{i_o}\right)+\sqrt{\left(\frac{i}{i_o}\right)^2+4}\right]\right\} + \frac{RT}{2F}\ln\left(1-\frac{i}{i_{as}}\right)-\frac{RT}{2F}\left(1+\frac{p^{o}_{H_2}i}{p^{o}_{H_2O}i_{as}}\right)+\frac{RT}{4F}\ln\left(1-\frac{i}{i_{cs}}\right) \quad [6]$$

Effect of Cr-poisoning on cathodic polarizations.—As mentioned before, the activation polarization (η_{act}) is a sum of the cathodic and anodic contributions. Yoon et al. showed that the activation polarization occurring at low fuel utilization is dominated by the cathodic contribution and the anodic contribution is negligible.[30] In this work, the anodic fuel composition (98 H_2 - 2% H_2O) simulated negligible fuel utilization under flooded condition, and therefore the total activation polarization can be approximated as due to the cathodic activation polarization ($\eta_{act,c}$)[17,30]

$$\eta_{act} = \frac{2RT}{F}\ln\left\{\frac{1}{2}\left[\left(\frac{i}{i_o}\right)+\sqrt{\left(\frac{i}{i_o}\right)^2+4}\right]\right\} \approx \eta_{act,c} = \frac{2RT}{F}\ln\left\{\frac{1}{2}\left[\left(\frac{i}{i_{o,c}}\right)+\sqrt{\left(\frac{i}{i_{o,c}}\right)^2+4}\right]\right\} \quad [7]$$

where $i_{o,c}$ is the cathodic exchange current density. Substituting Equation 7 in Equation 6, the C-V measurement can be modelled as

$$V_{cell}(i) = V_o - iR_i - \frac{2RT}{F}\ln\left\{\frac{1}{2}\left[\left(\frac{i}{i_{o,c}}\right)+\sqrt{\left(\frac{i}{i_{o,c}}\right)^2+4}\right]\right\} + \frac{RT}{2F}\ln\left(1-\frac{i}{i_{as}}\right)-\frac{RT}{2F}\left(1+\frac{p^{o}_{H_2}i}{p^{o}_{H_2O}i_{as}}\right)+\frac{RT}{4F}\ln\left(1-\frac{i}{i_{cs}}\right) \quad [8]$$

In the modeling, since the anode fuel composition and flow rate were fixed, it was assumed that the initial anodic saturation current density (i_{as}) would not change with time, and thus i_{as} obtained from the initial C-V curves were kept constant for modeling the Cr-poisoned cell performance. In addition, assuming the resistance of lead wire did not change, the difference of R_Ω measured by EIS (high-frequency intercept in impedance spectra) before and after Cr-poisoning (ΔR_Ω) was set to be equal to the difference of R_i (ΔR_i).

Using the above-mentioned assumptions, the short-term effects of Cr-poisoning on the cathode performance were evaluated. The C-V curves measured at 0 h (without Cr-poisoning effects) and 24 h (with Cr-poisoning effects) of Cell B and Cell D were fitted to the polarization model discussed previously in Equation 8 and are shown in Figure 4. The fitting parameters: area specific ohmic resistance (R_i), cathodic exchange current density ($i_{o,c}$), anodic saturation current density (i_{as}), and cathodic saturation current density (i_{cs}) obtained from the C-V curves of Cell B and D are listed in Table II.

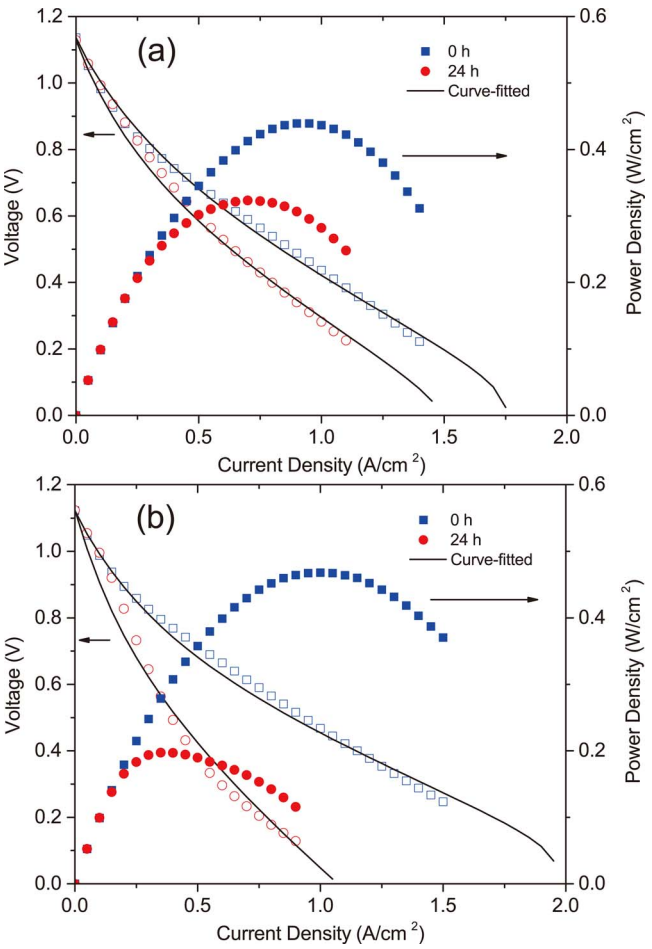

Figure 4. Cell test and polarization modeling results of the cells before and after 24 hours of 0.5 A/cm^2 cathodic current density: (a) with dry air (Cell B) and (b) with 10% humidified air (Cell D).

Table II. Curve fitting results of Cell B and Cell D before and after 24 hours of 0.5 A/cm^2 cathodic current.

	Cell B		Cell D	
Fitting Parameters	0 hour	24 hours	0 hour	24 hours
R_i (Ohm · cm^2)	0.169	0.127	0.112	0.104
$i_{o,c}$ (A/cm^2)	0.146	0.066	0.124	0.024
i_{as} (A/cm^2)	2.210	2.210	2.695	2.695
i_{cs} (A/cm^2)	1.760	1.505	1.970	1.078

In the polarization modeling results of both Cell B and D (see Table II), significant changes in cathodic exchange current density ($i_{o,c}$) were observed. After 24 hours of galvanostatic condition (at 0.5 A/cm^2), $i_{o,c}$ decreased from 0.146 to 0.066 A/cm^2 (by ∼55%) in Cell B, and it decreased from 0.124 to 0.024 A/cm^2 (by ∼81%) in Cell D. The cathodic exchange current density is a measure of the forward and reverse cathode reaction rates at equilibrium potential, and is associated with cathodic activation polarization through Equation 7. A high cathodic exchange current density means a high oxygen reduction reaction (ORR) rate at the cathode. Decreases in cathodic saturation current density (i_{cs}) were also found (see Table II). i_{cs} decreased from 1.760 to 1.505 A/cm^2 (by ∼14%) in Cell B, and it decreased from 1.970 to 1.078 A/cm^2 (by ∼45%) in Cell D. Cathodic saturation current density is a measure of diffusivity of the oxidant in the cathode, and is associated with the cathodic concentration polarization through Equation 5. A high cathodic saturation current density means a fast diffusion of oxygen from the bulk cathode to the cathode/electrolyte interface. A comparison between the microstructures of Cell B and Cell D (discussed in section Microstructures) also shows that the porosity in the cathode active layer in Cell D is significantly lower than that of Cell B due to the deposition of Cr-containing species, thus confirming the conclusion of the polarization modeling.

To evaluate the effects of Cr-poisoning on cathodic activation polarization ($\eta_{act,c}$) and cathodic concentration polarization ($\eta_{conc,c}$), it is important to quantitatively determine their impacts on cell performance degradation. Using the fitting parameters ($i_{o,c}$ and i_{cs}) in Equations 5 and 7, $\eta_{act,c}$ and $\eta_{conc,c}$ of Cell B and D before and after Cr-poisoning were calculated as functions of current density, and they are plotted in Figure 5. It was found that the increase of cathodic activation polarization was most dominant. Also, compared with the cell tested with dry air (Cell B), the increase of cathodic activation polarization was much higher in the cell tested with humidified air (Cell D). Under normal operating conditions, the effect of Cr-poisoning on the cathodic concentration polarization is negligible but near saturation current densities it can rapidly increase (see Figure 5).

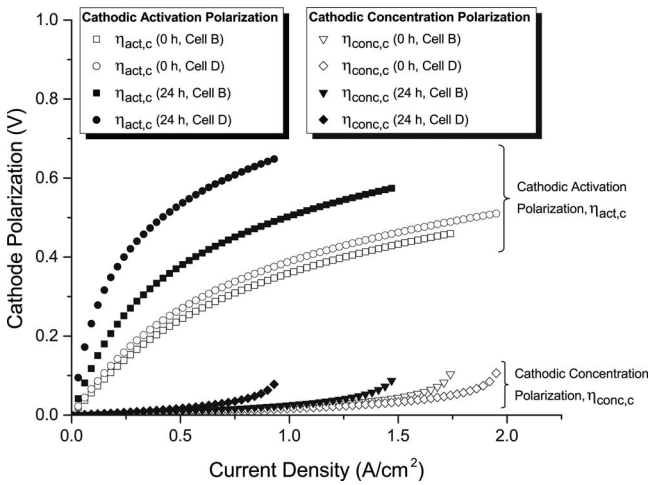

Figure 5. Cathodic activation polarization ($\eta_{act,c}$) and cathodic concentration polarization ($\eta_{conc,c}$) of Cell B and D before and after 24 hours of Cr-poisoning.

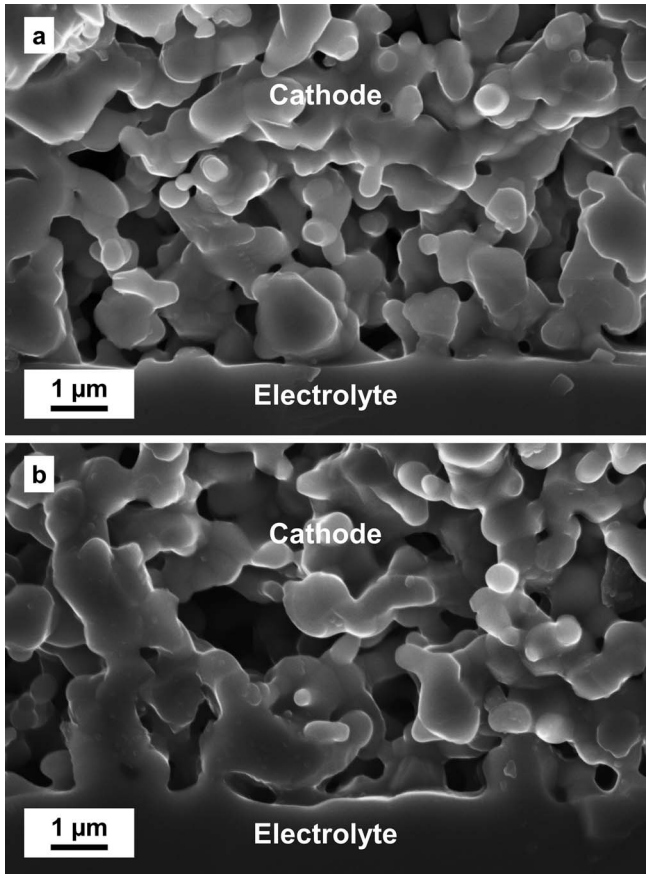

Figure 6. SEM micrographs of cathode cross sections in fractured cells: (a) Cell A: tested with dry air under open-circuit condition, and (b) Cell C: tested with 10% humidified air under open-circuit condition.

Microstructures.—SEM and EDX were used for the microstructure characterization of the cathode cross sections of the tested cells. Figure 6 shows the SEM micrographs of the cathode cross sections of Cell A and C (which are tested under open-circuit condition). No Cr-containing deposits were observed near the cathode/electrolyte interfaces in these two cells, which also corresponds to the stable cell performances mentioned in section Current-voltage measurements and Electrochemical impedance spectroscopy under open-circuit condition.

In Cell B and D which were tested under galvanostatic condition, Cr-containing deposits were observed (see Figure 7) which indicates that Cr deposition is electrochemically facilitated. In the case of Cell B (Figure 7a), a large amount of Cr-containing deposits having size of less than 100 nm were observed. These deposits were mainly located near the cathode/electrolyte interface (see Figure 7c). In the case of Cell D (Figure 7b), two types of Cr-containing deposits were observed in the cathode cross section: (a) clear crystals with distinct facets having size of around 500 nm near the cathode/electrolyte interface (see Figure 7d), and (b) smaller deposits having size of less than 100 nm (similar in morphology to those in Cell B) located at around 5–15 μm away from the electrolyte (see Figure 7e).

EDX analyses were used to examine the elemental changes in the cathode cross sections. When examining Cr-poisoned LSM samples by EDX analysis, two overlaps were commonly observed: between CrKα and LaLβ$_2$ peak, and between CrKβ and MnKα peak. For quantifying the concentration of Cr and Mn, the intensity of LaLα peak was taken as a reference since LaLβ$_2$/LaLα and MnKβ/LaLα are fixed in a Cr-free sample (for a fixed composition). Thus, the relative intensity ratio of the (LaLβ$_2$ + CrKα)/LaLα was taken as an effective criterion of the Cr deposition, and the relative intensity ratio of the

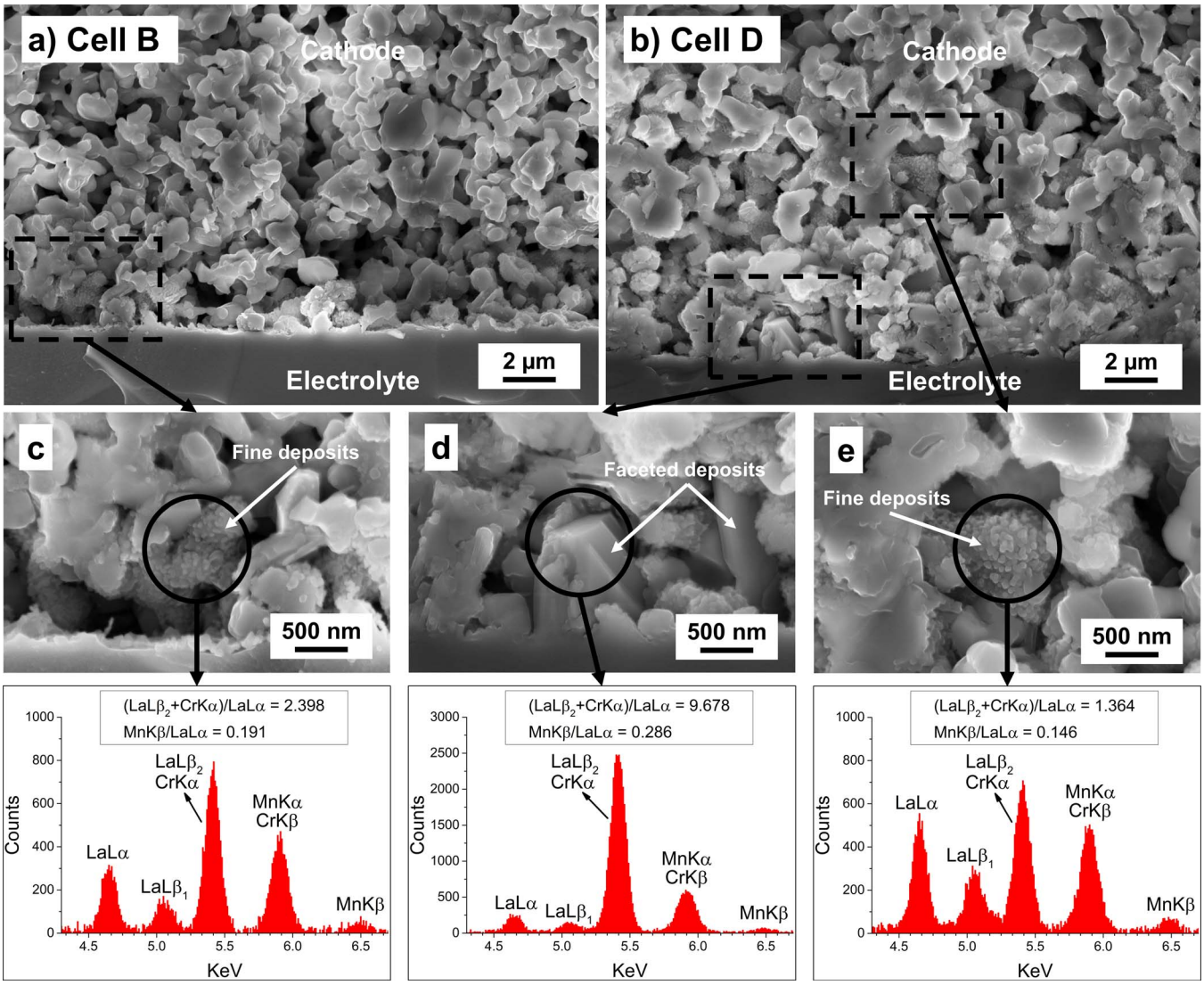

Figure 7. SEM micrographs of cathode cross sections in fractured cells and the corresponding EDX analyses in (a, c) Cell B: tested with dry air under 0.5 A/cm^2 cathodic current density, and (b, d, e) Cell D: tested with 10% humidified air under 0.5 A/cm^2 cathodic current density.

MnKβ/LaLα was taken as an effective criterion of the concentration of Mn. A larger (LaLβ$_2$ + CrKα)/LaLα or MnKβ/LaLα intensity ratio indicates a higher Cr or Mn concentration, respectively. In an untested Cr-free cell, the average LaLβ$_2$/LaLα intensity ratio was measured to be ∼0.171, and the average MnKβ/LaLα intensity ratio was measured to be ∼0.115.

Figure 7 also shows the EDX spectra collected for the Cr-containing deposits. The (LaLβ$_2$ + CrKα)/LaLα and MnKβ/LaLα intensity ratios of crystals with facets (see Figure 7d) and finer deposits (see Figures 7c and 7e) are higher than their baseline values in an untested Cr-free cell, indicating they are Cr and Mn rich phases. The intensities of Cr and Mn from the faceted crystals are much higher than those at the finer deposits, and this indicates that Mn in the LSM was getting depleted by the Cr-containing deposits near the cathode/electrolyte interface in the case of Cell D. These Cr and Mn rich faceted crystals are likely to be $(Mn,Cr)_3O_4$ spinels, which were also observed by many other researchers.[11,31–33] Compared with Cell B, presence of humidity in the case of Cell D played an important role in Cr-poisoning. At 800°C, the most abundant Cr-containing vapor species in dry air is CrO_3. In contrast, the most abundant Cr-containing vapor species in 10% humidified air is $CrO_2(OH)_2$ and its equilibrium partial pressure at 800°C is approximately 2 orders of magnitude higher than that of CrO3 in dry air.[7] The formation of large faceted deposits at cathode/electrolyte interface in Cell D is likely due to the significantly higher Cr vapor pressure in humidified air than that in dry air.

In order to quantify the amount of Cr-containing deposits at different cathode locations, EDX spectra were collected from rectangular areas (2 μm in the direction of cathode bulk and 16 μm parallel to the cathode/electrolyte interface) at 0, 1, 3, 5, 7, 15, 25, 40, 50 μm away from electrolyte, and the average intensity ratios of (LaLβ$_2$ + CrKα)/LaLα in these areas were obtained and compared. Figure 8 shows the (LaLβ$_2$+CrKα)/LaLα intensity ratios as functions of distance away from the electrolyte measured in the four tested cells. In the case of Cell A and C (tested under open-circuit condition), the (LaLβ$_2$ + CrKα)/LaLα intensity ratio is close to the baseline value throughout the cathode thickness. In the case of Cell B and D (tested under galvanostatic condition), however, concentration gradients of the amount of Cr-containing deposits ((LaLβ$_2$ + CrKα)/LaLα intensity ratio) are observed. The Cr concentration at the cathode/electrolyte interface are much higher than that in the bulk cathode in both Cell B and Cell D. Furthermore, the overall Cr concentration near the cathode/electrolyte interface in Cell D is much higher than that in Cell B, and the Cr-containing deposits in cell D extend more into the cathode compared

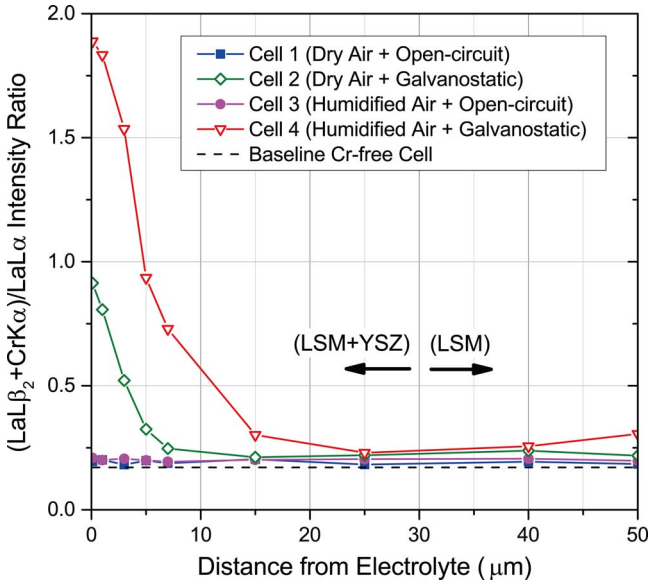

Figure 8. (LaLβ_2+CrKα)/LaLα intensity ratios measured at different cathode thicknesses, relative to the electrolytes of four tested cells.

with that in Cell B (agrees with the SEM observations). The possibility of minor surface diffusion of Cr-containing species from the Crofer22H mesh cannot be ruled out.[34] However, the Cr-poisoning at the cathode/electrolyte interface under galvanostatic conditions is clearly evident from Figure 8 (comparing Cell A with Cell B and Cell C with Cell D). Furthermore, in humidified air, the higher vapor pressure of the Cr-containing species magnifies the electrochemically induced Cr deposition and performance degradation (comparing Cell B with Cell D).

The observed overall composition profile in the cathode during Cr-poisoning in Cell B and D can be explained as follows. Initially the Cr-containing species are electrochemically deposited at the TPB's near the cathode/electrolyte interface. The Cr-containing deposits then start to deplete Mn from LSM near the cathode/electrolyte interface which results in the formation of Mn-Cr-O rich phases (likely $(Mn,Cr)_3O_4$ spinels). The Mn-depleted LSM and the LSM sites covered with Cr-containing deposits have less conductivity and catalytic activity for oxygen reduction reaction than the pristine LSM sites, resulting in the increase of cathode activation polarization. As a result, the TPB sites for charge transfer extend into the cathode and the Cr-containing deposits begin to appear in the cathode away from the electrolyte.

Conclusions

In this work, anode-supported solid oxide fuel cells with LSM-based cathode were electrochemically tested in direct contact with the Crofer22H mehses at 800°C, under different cathode atmospheres (dry air or humidified air) and current conditions (open-circuit or galvanostatic). When there was no cathodic current (Cell A and C), no performance degradation was observed during the 120-h testing and the cathode/electrolyte was found to be clean. However, in the presence of a constant 0.5 A/cm^2 cathodic current, significant performance degradations of the cells were observed and large amounts of Cr-containing deposits were found in the cathode cross sections. The degradation was found to be more severe when cathode was in 10% humidified air, compared with that in dry air.

Employing a polarization model, the electrochemically measured current-voltage curves before and after the Cr-poisoning were analyzed. The total polarization loss of a cell is separated into the contributions of cathodic activation polarization, cathodic concentration polarization, anodic concentration polarization and ohmic polarization. It is determined for the first time that the performance degradation caused by Cr-poisoning is primarily due to the significant increase of the cathodic activation polarization, and it is considered to be due to the decreasing electrochemically active sites for oxygen reduction reaction near the cathode/electrolyte interface. Cathodic concentration polarization also increases due to Cr-poisoning because the Cr-containing deposits aggregate within the pores of the cathode and block the gas diffusion, but this effect is less prominent than the increase of cathodic activation polarization. This study quantitatively shows the effects of Cr-poisoning on different cathodic polarization losses and the observations correlate well with the microstructural changes in the cathode.

Acknowledgments

Financial support from U. S. Department of Energy, Office of Fossil Energy, through Award # FE0023325 is gratefully acknowledged.

References

1. L. Blum, W. A. Meulenberg, H. Nabielek, and R. Steinberger-Wilckens, *Int. J. Appl. Ceram. Technol.*, **2**(6), 482 (2005).
2. R. Gemmen and C. Johnson, *J. Power Sources*, **159**(1), 646 (2006).
3. H. Yokokawa, H. Tu, B. Iwanschitz, and A. Mai, *J. Power Sources*, **182**(2), 400 (2008).
4. S. Badwal, R. Deller, K. Foger, Y. Ramprakash, and J. Zhang, *Solid State Ionics*, **99**(3), 297 (1997).
5. T. Horita, Y. Xiong, H. Kishimoto, K. Yamaji, M. E. Brito, and H. Yokokawa, *J. Electrochem. Soc.*, **157**(5), B614 (2010).
6. S. P. Jiang and X. Chen, *Int. J. Hydrogen Energy*, **39**(1), 505 (2014).
7. R. Wang, M. Würth, B. Mo, U. B. Pal, S. Gopalan, and S. N. Basu, *ECS Trans.*, **75**(42), 61 (2017).
8. S. Taniguchi, M. Kadowaki, H. Kawamura, T. Yasuo, Y. Akiyama, Y. Miyake, and T. Saitoh, *J. Power Sources*, **55**(1), 73 (1995).
9. E. Konysheva, J. Mertens, H. Penkalla, L. Singheiser, and K. Hilpert, *J. Electrochem. Soc.*, **154**(12), B1252 (2007).
10. J. J. Bentzen, J. V. T. Høgh, R. Barfod, and A. Hagen, *Fuel Cells*, **9**(6), 823 (2009).
11. M. Krumpelt, T. A. Cruse, B. J. Ingram, J. L. Routbort, S. Wang, P. A. Salvador, and G. Chen, *J. Electrochem. Soc.*, **157**(2), B228 (2010).
12. M. J. Jørgensen and M. Mogensen, *J. Electrochem. Soc.*, **148**(5), A433 (2001).
13. R. Barfod, M. Mogensen, T. Klemensø, A. Hagen, Y. -L. Liu, and P. V. Hendriksen, *J. Electrochem. Soc.*, **154**(4), B371 (2007).
14. Y. Matsuzaki and I. Yasuda, *Solid State Ionics*, **132**(3), 271 (2000).
15. M. Kornely, A. Neumann, N. H. Menzler, A. Leonide, A. Weber, and E. Ivers-Tiffée, *J. Power Sources*, **196**(17), 7203 (2011).
16. A. Bieberle and L. Gauckler, *Solid State Ionics*, **146**(1), 23 (2002).
17. K. J. Yoon, S. Gopalan, and U. B. Pal, *J. Electrochem. Soc.*, **154**(10), B1080 (2007).
18. B. Kuhn, C. A. Jimenez, L. Niewolak, T. Hüttel, T. Beck, H. Hattendorf, L. Singheiser, and W. Quadakkers, *Mater. Sci. Eng., A*, **528**(18), 5888 (2011).
19. J. Bauerle, *J. Phys. Chem. Solids*, **30**(12), 2657 (1969).
20. A. Barbucci, R. Bozzo, G. Cerisola, and P. Costamagna, *Electrochim. Acta*, **47**(13), 2183 (2002).
21. K. J. Yoon, S. Gopalan, and U. B. Pal, *J. Electrochem. Soc.*, **156**(3), B311 (2009).
22. S. Jiang, J. Zhang, and K. Foger, *J. Electrochem. Soc.*, **147**(9), 3195 (2000).
23. X. Chen, Y. Zhen, J. Li, and S. P. Jiang, *Int. J. Hydrogen Energy*, **35**(6), 2477 (2010).
24. S. Jiang and J. Love, *Solid State Ionics*, **138**(3), 183 (2001).
25. K. J. Yoon, P. Zink, S. Gopalan, and U. B. Pal, *J. Power Sources*, **172**(1), 39 (2007).
26. J. W. Kim, A. V. Virkar, K. Z. Fung, K. Mehta, and S. C. Singhal, *J. Electrochem. Soc.*, **146**(1), 69 (1999).
27. S. Chan, K. Khor, and Z. Xia, *J. Power Sources*, **93**(1), 130 (2001).
28. K. J. Yoon, W. Huang, G. Ye, S. Gopalan, U. B. Pal, and D. A. Seccombe, *J. Electrochem. Soc.*, **154**(4), B389 (2007).
29. P. Li and M. Chyu, *J. Heat Transfer*, **127**(12), 1344 (2005).
30. K. J. Yoon, S. Gopalan, and U. B. Pal, *J. Electrochem. Soc.*, **155**(6), B610 (2008).
31. S. Wang, T. Cruse, M. Krumpelt, B. Ingram, and P. Salvador, *J. Electrochem. Soc.*, **158**(2), B152 (2011).
32. S. P. Jiang, Y. Zhen, and S. Zhang, *J. Electrochem. Soc.*, **153**(8), A1511 (2006).
33. D. Röhrens, A. Neumann, A. Beez, I. Vinke, L. de Haart, and N. Menzler, *Ceram. Int.*, **42**(8), 9467 (2016).
34. M. C. Tucker, H. Kurokawa, C. P. Jacobson, L. C. De Jonghe, and S. J. Visco, *J. Power Sources*, **160**(1), 130 (2006).